Robust integer and fractional helical modes in the quantum Hall effect

Yuval Ronen[†]*, Yonatan Cohen*[†]*, Daniel Banitt, Moty Heiblum*[#] *and Vladimir Umansky*
Braun Center for Submicron Research, Department of Condensed Matter Physics,
Weizmann Institute of Science, Rehovot 76100*, Israel*

[†] *equal contributions*

[#] *corresponding author* (moty.heiblum@weizmann.ac.il)

Supplementary information

We add here details and complementary measurements that could not find room in the main text. In section S1 we demonstrate the importance of a double well configuration for obtaining ballistic helical modes. In sections S2 & S3 we present additional measurements and further analysis of the integer and fractional helical states. In section S4 we show measurements of counter-propagating edge modes of integer and fractional states; specifically in the ν=1 and ν=1/3 states; as well as evidence for mixing (tunneling) between them. And finally in section S5 we present measurements that are performed on a wider quantum well (without an AlAs barrier in the middle), where stronger tunneling between the edge modes in the two sub-bands is present; and finally,

S1. Counter propagating edge modes with a single 2DEG

In Fig. S1, three different configurations illustrate the necessity of two sub-bands in the quantum Hall effect regime for obtaining counter-propagating edge modes with opposite spins, *i.e.* helical modes.

S2. Complementary measurements of integer helical states

Figure S2 shows measurements of the reflected and transmitted currents at contacts D_1 and D_2, respectively, for a current sourced from contact S_1. Evidently, the currents have little to no

dependence on the counter-propagation length, L_{CP}, when the edge modes have opposite spins, such as at $(4,0)\rightarrow(3,1)$ and $(6,0)\rightarrow(5,1)$ (Figs. S2a & S2b). In contrast, when spin protection is lifted, such as at $(3,0)\rightarrow(2,1)$ and $(5,0)\rightarrow(4,1)$, there is a significant dependence on the length (Figs. S2c & S2d). It is important to note that as the propagation length increases, the decrease in $I_{S1\rightarrow D1}$ is exactly compensated by an increase in $I_{S1\rightarrow D2}$ (consistently summing up to the injected current). Evidently, the change in the currents is due to tunneling between edge modes and not due to finite bulk conductance. Figure S2e summarizes the mean transmission coefficient across the plateau, with standard deviations (STD) error bars, of the reflected current as function of the propagation length for different spin configurations. Significant inter-mode tunneling is found when the counter propagating edge modes have the same spin (red and magenta); with characteristic decay lengths of order of millimeters. For helical modes (blue and green), no measurable decay is observed.

S3. Complementary measurement of fractional helical state

As seen in Fig. S3a, in the fractional quantum Hall regime an observed reduction in the reflected current, $I_{S1\rightarrow D1}$, with increasing the propagation length is observed. However, there is no corresponding increase in the transmitted current, $I_{S1\rightarrow D2}$. Moreover, as shown in Fig. S3b, a non-zero R_{XX} is found in the right half-plane in the corresponding gate voltage range. Therefore, we attribute the decrease in the reflected current to current flow through the bulk (and to other grounded contacts) rather than to tunneling between the edge modes. Note that this is consistent with the fact that when current is injected from contact S_2, the reflected current $I_{S2\rightarrow D2}$ is not affected by the length of propagation.

S4. Counter propagating integer and fractional edge modes

Figure S4 shows a mixed case of 'integer-fractional' modes, were the filling on the right varies from $(1,0)$ to $\left(\frac{4}{3},0\right)$ ending in $(1,1)$, while the left side is kept at $(1,1)$. In the case of $\left(\frac{4}{3},0\right)\rightarrow(1,1)$, there is a biased edge mode with conductance of $\frac{1}{3}\frac{e^2}{h}$ counter propagating

alongside an integer $\frac{e^2}{h}$ edge mode. As the propagation length increases, the expected reflection of a quarter of the current, when propagation is ballistic, is suppressed (while transmission intensifies), indicating an increased tunneling of $e^* = \frac{1}{3}e$ quasiparticles into the integer mode carrying electrons.

S5. Wide quantum well structure (no internal barrier)

In a wide well structure, two sub-bands are populated with an increased spatial overlap between their wave-functions (here, the calculation is done with a certain gate voltage applied, to show the worst case of tunneling). One expects more significant inter-mode (inter sub-band) tunneling taking place.

Figure S5 presents measurement results in a 57nm wide QW. Two devices were measured with propagation lengths of 7 and $20\,\mu m$. A significant reduction from the ballistic behavior was found under the helical condition, $(6,0)\rightarrow(5,1)$ (marked by a red dotted line in Fig. S4b), even for propagation length of $7\,\mu m$. The deviation from zero in the $(6,0)\rightarrow(6,0)$ scenario is a result of finite Rxx. These results demonstrate that a reduction of the barrier thickness in the design of the quantum well structure will increase the tunneling between the counter propagating edge modes, and thus it can be well controlled.

Figure captions:

Fig. S1. Single sub-band with different filling factors. a, Upper panel: two isolated 2DEGs in filling factor 1 (with a groove between the two sides). Bottom panel: Top view of the sample showing two counter propagating edge modes with the same spin. **b,** Upper panel: a single sub-band 2DEG where the left side is in filling 2 and the right is in filling 1. Bottom panel: Top view of the sample showing a single edge mode reflecting (no groove between the two sides). **c,** Upper panel: two isolated 2DEGs, the left in filling 2 and the right in filling 1 (with a groove between the two sides). Bottom panel: Top view of the sample showing the edge modes configuration.

Fig. S2. Propagation length in different spin configurations at the IQHE. a-d, Reflected (top) and transmitted (bottom) currents in the integer fillings. The percentage written (near each arrow, which indicate an increase or decrease) express the difference between the current measured when the propagation length L_{CP} was $300\,\mu m$ and $7\,\mu m$. **e,** Mean transmission of the biased edge mode for each of the measured fillings, as function of the propagation length. The corresponding characteristic decay length ξ (in order of mm) assumes an exponential decay with length. Error bars where calculated via standard deviations (STD) of the measured signal.

Fig. S3. Analysis of the fractional helical state configuration. a, Reflected (top) and transmitted (bottom) currents at a fractional configuration of filling $\left(\frac{4}{3},0\right)\rightarrow\left(1,\frac{1}{3}\right)$, manifests fractional helical edge modes of $e^{*}=\frac{1}{3}e$. The decrease in reflected current with respect to the propagation length is an order of magnitude larger than the corresponding increase in the transmission. **b,** The longitudinal resistance, *Rxx*, in the left and right sides of the sample as a function of the left gate voltage V_{LG} and the right gate voltage V_{RG}. The black arrow marks the value of V_{LG}, which was used to obtain the data in Fig. S2a, corresponding to filling $\left(\frac{4}{3},0\right)$. The

green region in **a**, corresponds to filling $\left(1,\frac{1}{3}\right)$ in the left side of the sample, correspond to the dotted box in **b**, exhibiting finite $R_{XX}\sim 40\text{ohm}$.

Fig. S4. Counter propagating integer and fractional edge modes. Reflected (top) and transmitted (bottom) coefficients in a mixed 'fractional-integer' case, with filling $\left(\frac{4}{3},0\right)\rightarrow(1,1)$. The fractional edge mode, with conductance $\frac{1}{3}\frac{e^2}{h}$, is biased, counter propagating along an integer edge mode. The percentage difference between the current measured when the propagation length was $300\,\mu m$ compared to that of the $7\,\mu m$ is written next to an arrow indicating the direction of change (increase or decrease).

Fig. S5. Typical measurements of a 57nm wide QW. a, Rxx measurement. **b,** Zoom-in Rxx measurement on the $(6,0)\rightarrow(5,1)$ transition - marked by the dashed black box in Fig S5a. The red dotted line indicates the magnetic field at which the measurement shown in Fig S5c was conducted. **c,** Measurement of the voltage on the reflected edge. Black arrows indicate the location of FF $(6,0)\rightarrow(5,1)$ for each of the devices were a fully reflected edge mode is expected. The deviation from expected value, marked by a dotted line, even in short propagation lengths, indicates stronger tunneling between edge modes compared to the structure described in the main text. In the regime of $(6,0)\rightarrow(6,0)$ a zero current (resistance) is expected however finite R_{XX} gives rise to reflections not related to the edge modes. **d,** A simulation of a wide QW potential landscape and the first two subbands.

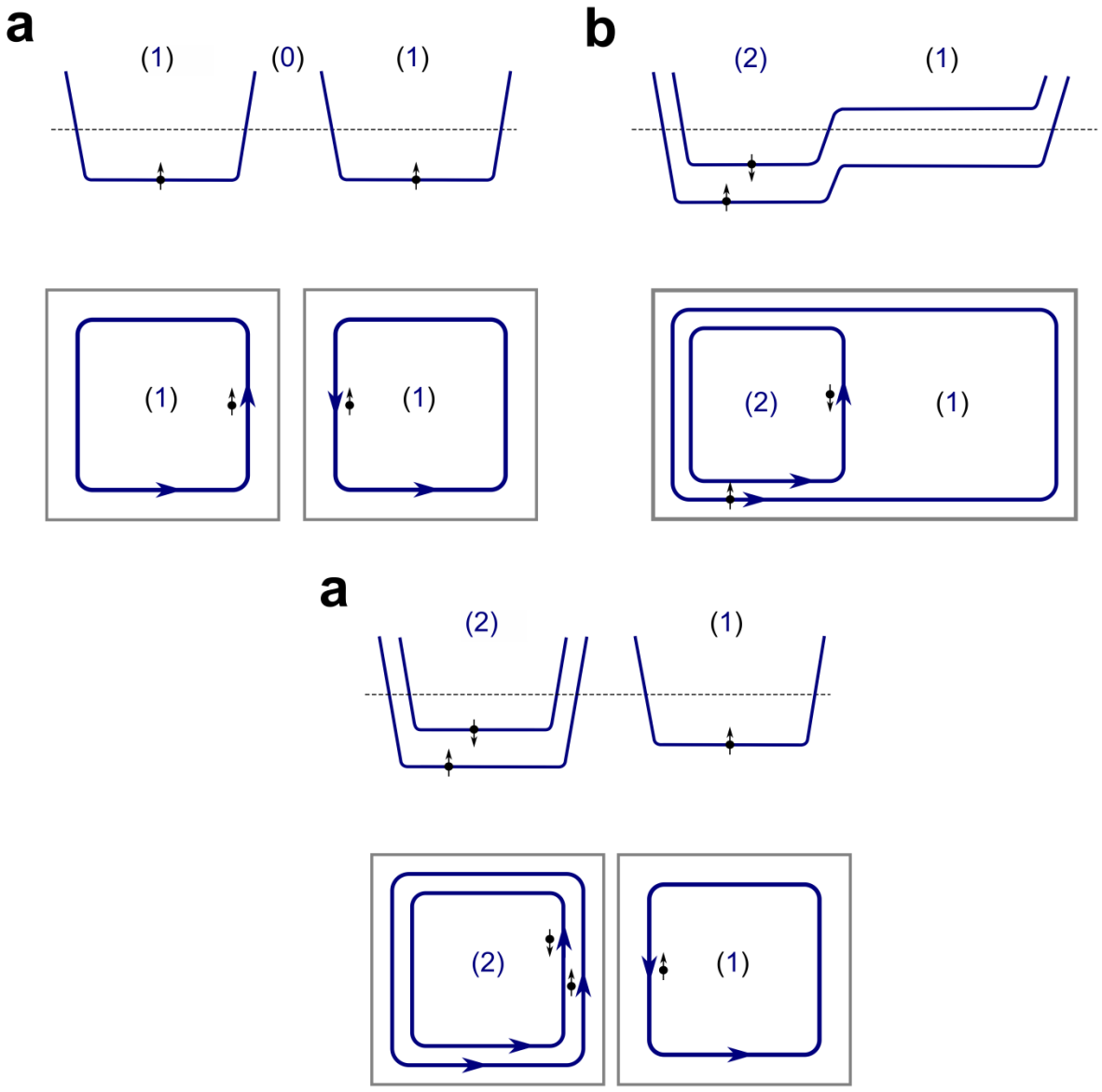

Fig S1

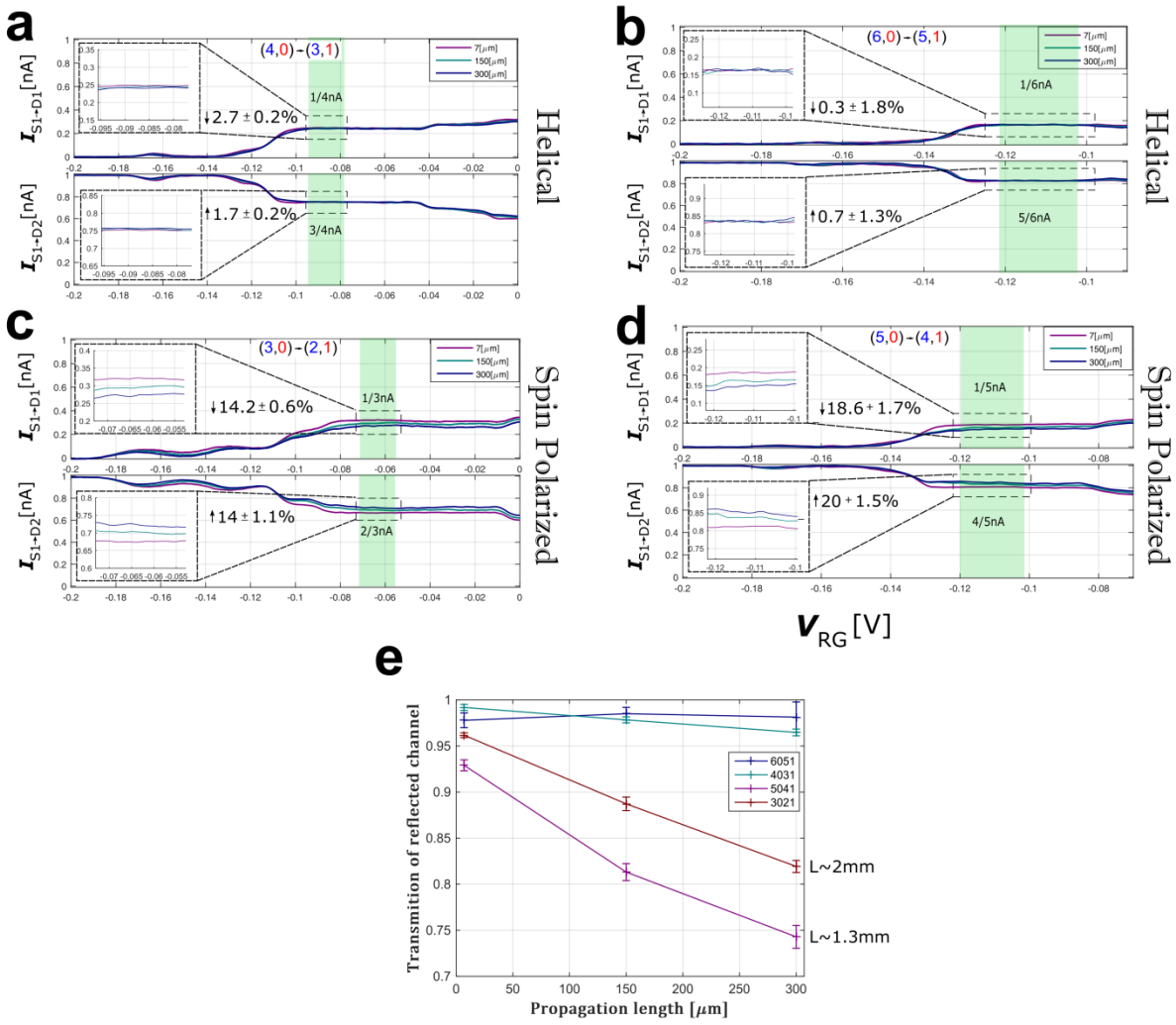
a
b
c
d
e
(4,0)-(3,1)
(6,0)-(5,1)
(3,0)-(2,1)
(5,0)-(4,1)
7[μm]
150[μm]
300[μm]
↓2.7±0.2%
1/4nA
↑1.7±0.2%
3/4nA
↓0.3±1.8%
1/6nA
↑0.7±1.3%
5/6nA
↓14.2±0.6%
1/3nA
↑14±1.1%
2/3nA
↓18.6+1.7%
1/5nA
↑20+1.5%
4/5nA
Helical
Spin Polarized
$I_{S1\text{-}D1}$[nA]
$I_{S1\text{-}D2}$[nA]
V_{RG}[V]
Transmition of reflected channel
Propagation length [μm]
6051
4031
5041
3021
L~2mm
L~1.3mm

Fig S2

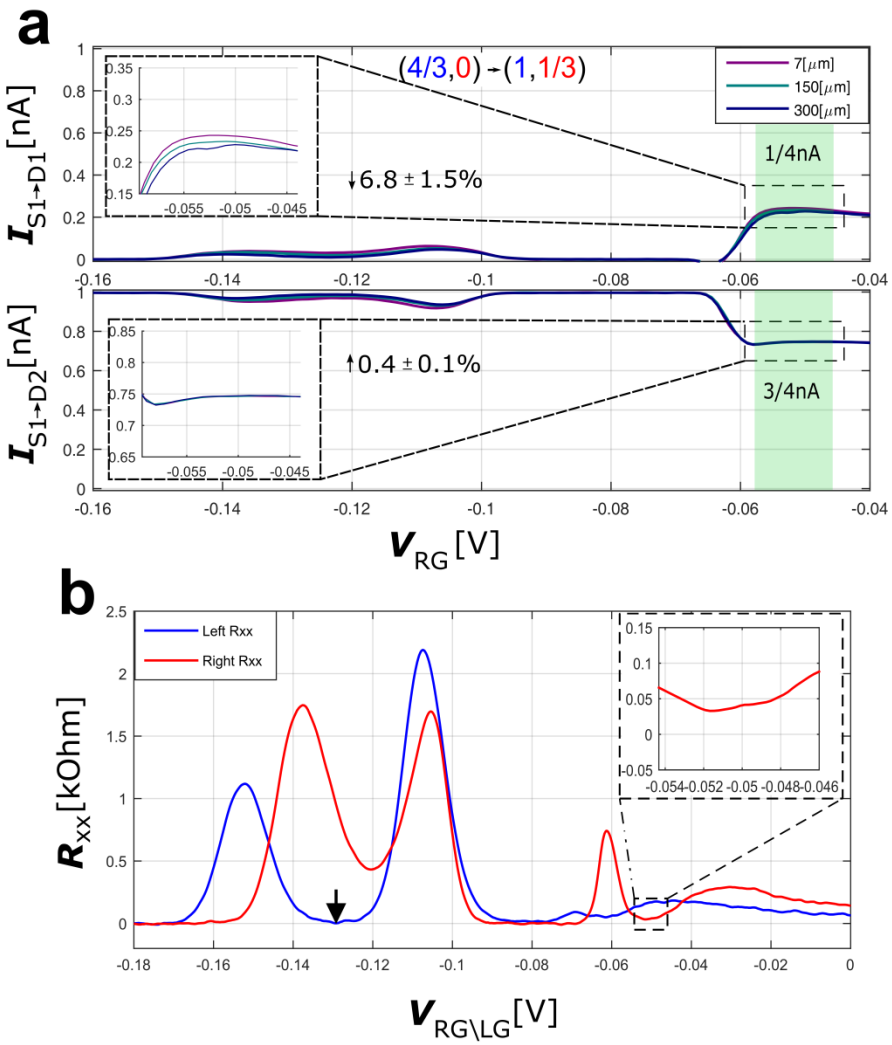
a
(4/3,0)→(1,1/3)
7[μm]
150[μm]
300[μm]
1/4nA
↓6.8 ± 1.5%
↑0.4 ± 0.1%
3/4nA
$I_{S1\to D1}$[nA]
$I_{S1\to D2}$[nA]
V_{RG}[V]
b
Left Rxx
Right Rxx
R_{xx}[kOhm]
$V_{RG\backslash LG}$[V]

Fig S3

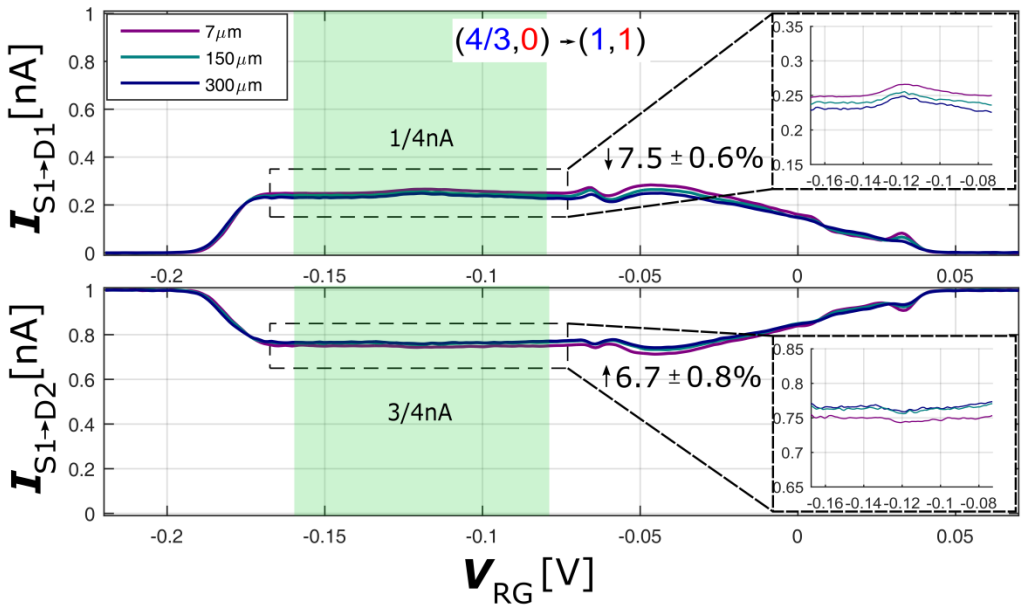
7μm
150μm
300μm
(4/3,0) → (1,1)
1/4nA
↓7.5 ± 0.6%
3/4nA
↑6.7 ± 0.8%
$I_{S1\to D1}$[nA]
$I_{S1\to D2}$[nA]
V_{RG}[V]

Fig S4

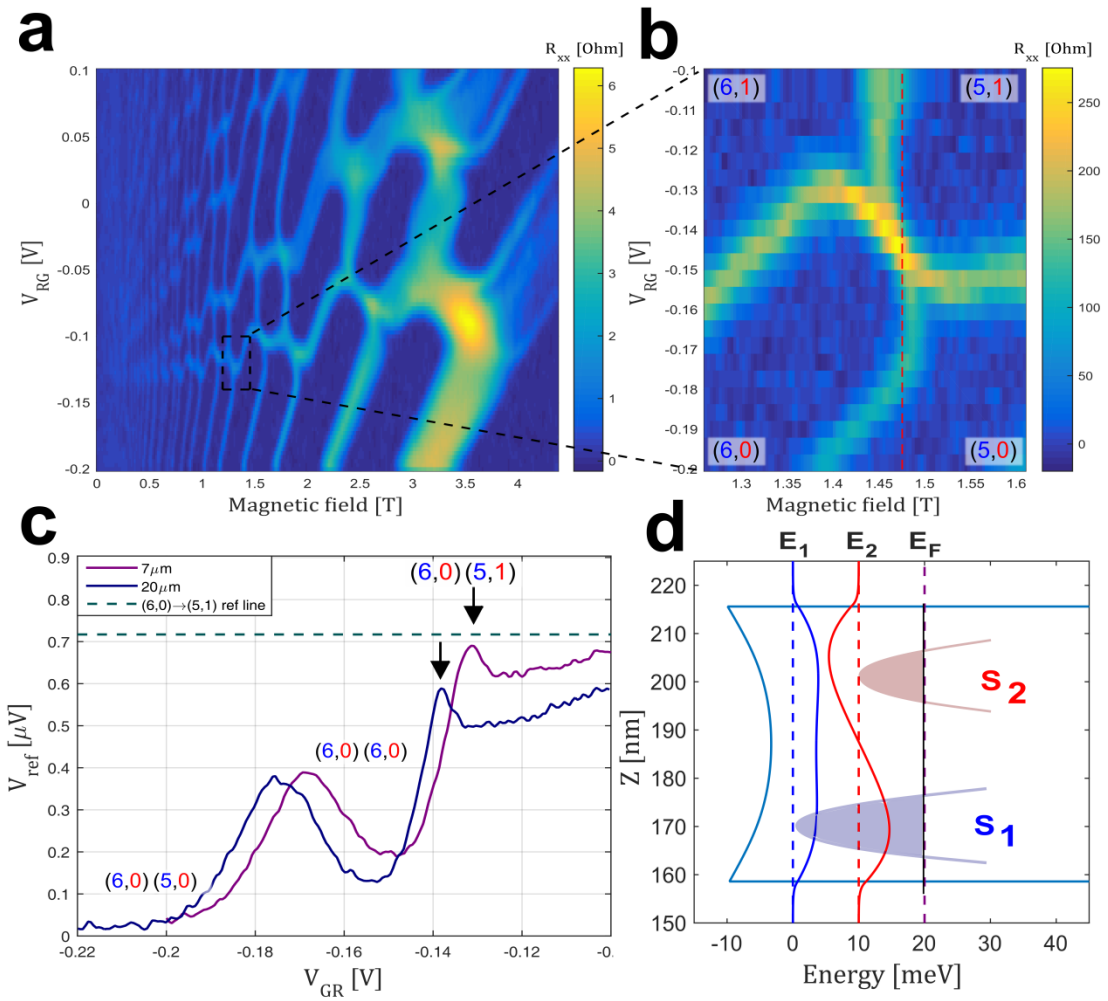
a
b
c
d
R_xx [Ohm]
V_RG [V]
Magnetic field [T]
(6,1)
(5,1)
(6,0)
(5,0)
7μm
20μm
(6,0)→(5,1) ref line
(6,0) (5,1)
(6,0) (6,0)
(6,0) (5,0)
V_ref [μV]
V_GR [V]
E_1
E_2
E_F
S_2
S_1
Z [nm]
Energy [meV]

Fig S5